Pergamon

Cement and Concrete Research 30 (2000) 981–987

CEMENT AND CONCRETE RESEARCH

Communication

# Reconstruction and analysis of 3-D profile of fracture surface of concrete

Ke-Ru Wu*, An Yan, Juan-yu Liu, Dong Zhang, Wu Yao

*State Key Laboratory of Concrete Materials Research, Tongji University, 1239 Siping Road, Shanghai 200092, People's Republic of China*

Received 15 October 1999; accepted 2 March 2000

**Abstract**

A new experimental technique based on laser triangulation to analyze and reconstruct 3-D fracture surfaces of concrete was proposed. Results of the reconstruction of a standard object and of the fracture surface of a concrete specimen showed that this technique has reasonable accuracy. Compared with the traditional analysis methods, this method is very convenient to determine the fractal dimension and other parameters of fracture surfaces, since indirect or destructive experimental procedures that are laborious and time-consuming are avoided. Quantitative analysis of roughness and the fractal feature of the fracture surface of concrete was also carried out. According to the value of roughness parameter $R_s$ (i.e. the ratio of actual surface area to projected surface), it is shown that the true fracture surface area is about 45.4% greater than the nominal fracture area. Two methods of calculation of fractal dimension, i.e. modified slit-island technique and vertical section analysis, were employed and preliminary analysis results indicated that the fracture surface of concrete is fractal, with fractal dimension ranging from 2.1 to 2.2. This new technique may be of great help to precisely measure fracture parameters and eventually improve our understanding of failure mechanisms of concrete. 

*Keywords:* Image analysis; Surface area; Mechanical properties; Concrete; 3-D profile

## 1. Introduction

As important post-mortem evidence, the fracture surface helps to reveal the micromechanisms of fracture and plays an essential part in the evaluation of fracture mechanics properties of cementitious materials. How to study the nature and characteristics of fracture surfaces has become an important research area in materials science and fracture mechanics.

Due to the limitations of previous experimental methods, the fracture surfaces were often simply idealized as 2-D planes in the fracture mechanics research of quasi-brittle materials such as concrete, which impaired the validity of measured fracture parameters, and even resulted in incorrect conclusions [1–3]. Furthermore, much valuable information about the micro- and meso-structure and failure mechanisms reflected in the fracture surfaces of materials was ignored. Thus, how to correctly and quantitatively measure the fracture surface of concrete remains an important problem to be solved.

Since the celebrated work of Mandelbrot et al. [4], fractal geometry has been widely used to characterize and model rough surfaces of various materials. There are various definitions of the fractal dimension of an object, including the Hausdorff dimension, the Bouligand–Minkowski dimension, the box-counting dimension and others. In fact, different techniques to extract the fractal dimension of a fracture surface can be developed, based on different definitions. However, conventional methods such as the slit-island method [4] and the vertical profile method [5] would destroy the fracture surfaces, which makes checking the results impossible and destroys the microstructure of fracture surfaces, hence impairing the measurement accuracy. Other methods [6–8] are time-consuming and have low accuracy due to the drawbacks of experimental equipment or limitation of computer hardware, though they enable the nondestructive analysis of fracture surface of concrete. Using 3-D stereo pairs [9] and structural light projection methods [10] to acquire shape features of fracture surfaces of concrete based on optics theory are new breakthroughs. However, it is still difficult to reconstruct the 3-D profile due to complicated calculations, since surface texture is a major focus of fractography.

Hence, this paper represents an attempt to reconstruct the 3-D profile of the fracture surface of concrete using

* Corresponding author. Tel.: +86-21-659-82412; fax: +86-21-659-83465.

*E-mail address*: wukeruk@online.sh.cn (K.R. Wu).

0008-8846/00/$ – see front matter 
PII: S0008-8846(00)00249-0

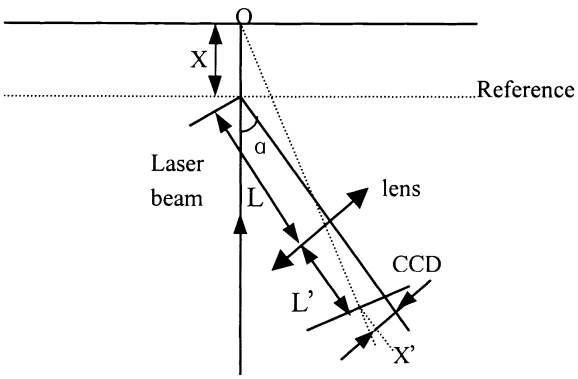


Fig. 1. Mechanism of laser triangulation.

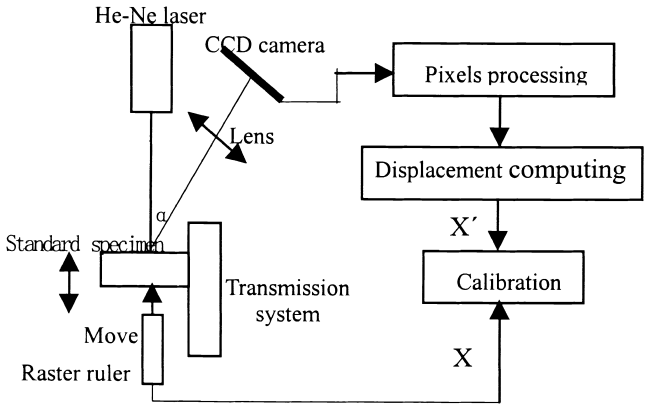


Fig. 3. Calibration of laser triangulation.

laser triangulation and an image grabbing and processing setup, in order to acquire further understanding of the fracture surface of concrete. Then, quantitative analysis of fractal features and roughness of fracture surfaces of concrete can be carried out and the shape properties of a fracture surface can be quantified, which may be of great help to measure fracture parameters more precisely and eventually to improve our understanding of the failure mechanisms of concrete.

## 2. Experimental procedure

### 2.1. Principle of laser triangulation

The principle of laser triangulation [11] is shown in Fig. 1. A laser beam is projected onto one dot of the object surface. In another direction, the image of this light dot is received by the CCD camera. When the object moves, the position of the speckle on its surface changes. Accordingly, the position on the CCD camera changes. The relationship between these two is Eq. (1):

$$X = \frac{X'L}{L'\sin\alpha - X'\cos\alpha} \tag{1}$$

where, $X$, $X'$ are the real displacement of the object and the displacement of the speckle on the CCD camera, respectively; $L$, $L'$, $\alpha$ are structural parameters and are determined by specified requirement. So, by accurately measuring $X'$, the displacement of the object is acquired.

### 2.2. Experimental setup

As shown in Fig. 2, the experimental setup consists of three parts: (1) optical system, including an He–Ne laser, lenses, and a space filter; (2) transmission system, including a step-motor, a PLC, a sliding table, a derailleur, a gimbal and a switch; and (3) imaging system, including a CCD camera, a METOR/PPB image grabber, and a Pentium II-350 computer.

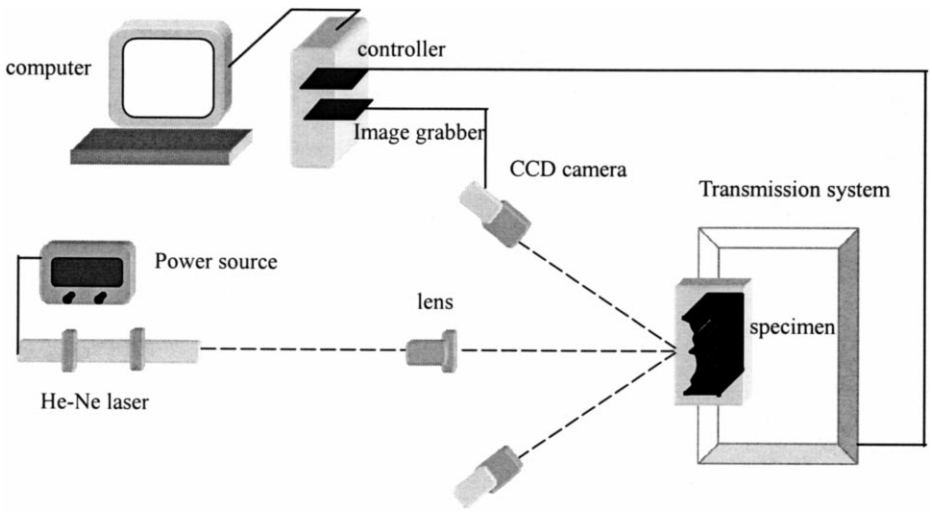


Fig. 2. Experimental setup.

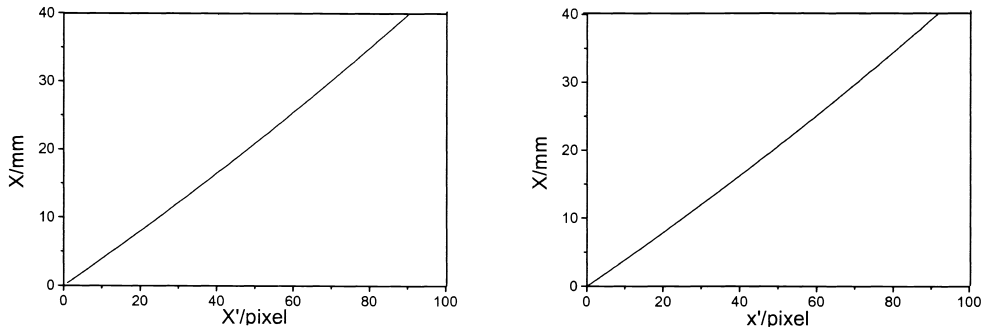


Fig. 4. Calibration curve.

After being expanded and collimated by lenses, the collimated light of an He–Ne laser beam (thickness = 0.2 mm) is projected onto the object surface and a contour line appears, whose image can be received by the CCD camera from a slanted direction. The sliding table with the specimen is controlled by the transmission system to move along the specified direction at a fixed speed (in this study, the speed was 1.6 mm/s), which enables the simultaneous scanning of projected light on the object surface. Through controlling the sampling interval of the image grabber (in this experiment, the image grabber grabbed eighth frame, the total number of frames was 200), the moving speed of the specimen is matched to the image-grabbing speed to achieve the timely grabbing of images. Due to different depths on the object surface, the image of every contour line on the photosensitive plane of the CCD camera is a curve. The real depths of the object surface can be obtained by calculating the offset of every image pixel on the curve compared to the reference plane.

### 2.3. Experimental setup parameters and calibration

The selection of setup parameters such as object distances, image distance, focus, the angle of $\alpha$ and so on is of great importance to the accuracy of the results. Longer object distances can expand the measurement range, while reducing the resolution. A longer image distance can improve the resolution, while reducing the measurement range and increasing the probe size. The optimal measurement can be achieved by properly choosing elements and structural size [12]. In this experiment, the probe parameters with a focus of 12 mm, object displacement of 26 mm, and image displacement of 22.3 mm could meet the demands of resolution and measurement range simultaneously.

Due to the roughness of the object surface, the contour line may become discrete when observed from a slanted direction. So a blind area is unavoidable during the measurement. The reason that the camera was used from two symmetrical directions was to compensate for the lack of image data, because a part of the slit image was lacking due to the shadow of the crack itself. Considering the blind area, the degree of $\alpha$ may be not too high, though it is suitable to increase the angle of $\alpha$ to reduce the noise of scattering speckles [13]. In this experiment, the angle of $\alpha$ was 30.

Formula (1) indicates that the relationship between $X$ and $X'$ is nonlinear. Though the three related structural parameters are fixed, it is very difficult to obtain the precise values during the course of manufacture and assembly. Hence, it is imperative to determine the relationship between $X$ and $X'$ through calibration. Fig. 3 illustrated the calibration process. The raster ruler was adopted to obtain the original data. The standard specimen was placed on the sliding table. The position of $X$ of 0.0 mm was determined

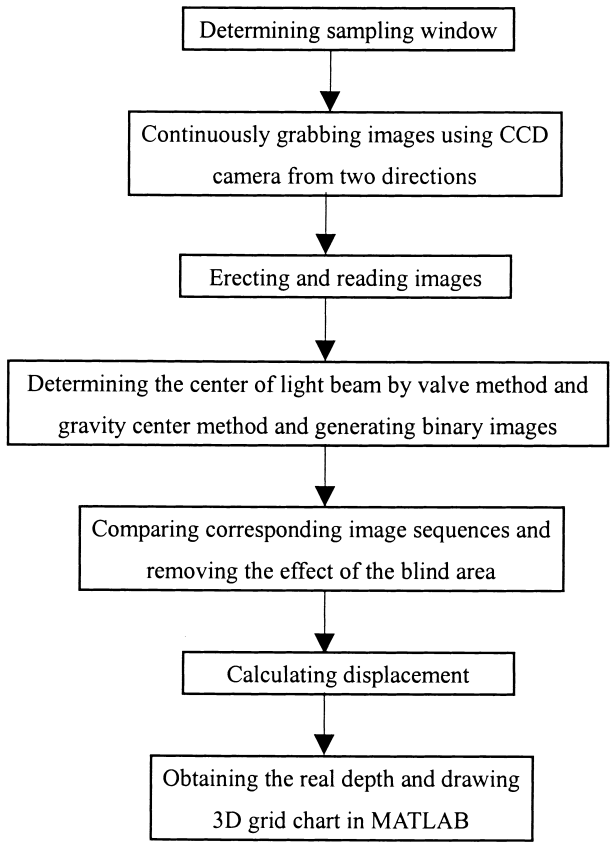


Fig. 5. The flow chart of image grabbing, processing, and data transformation.

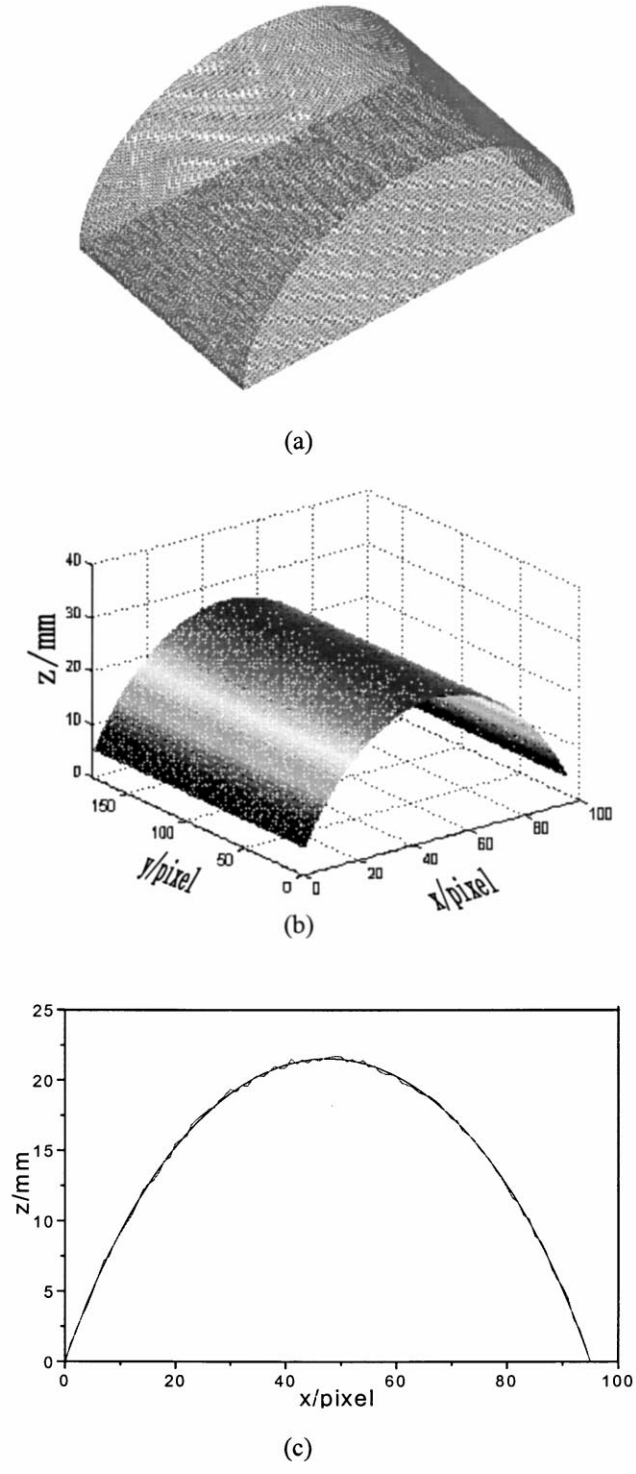


Fig. 6. Profile measurement of the standard work piece.

by moving the sliding table and the raster ruler was reset, i.e. the position of $X'$ of 0.0 mm was determined. Then, the sliding table was moved toward the direction of the value of $X'$ which was larger than 0 and the value of $X$ at that time was recorded. The results approximated by using a second order polynomial are illustrated in Fig. 4. The calibration equations were [Eqs. (2 and 3)].

$$X = 0.0006X'^2 + 0.3722X' + 0.0589, \quad (2)$$

$$X = 0.0006X'^2 + 0.3786X' + 0.0818. \quad (3)$$

The surplus (i.e. the difference between the displacements calculated by the above two calibration equations and the displacements measured by the raster ruler) was less than 0.1232 mm, which showed the reliability of the calibration results.

### 2.4. Image grabbing, processing, and data transformation

Image processing and data transformation were completed by using advanced software and analytical procedures. The flowchart is shown in Fig. 5.

### 2.5. Validity test

The profile of a work piece was reconstructed to examine the experimental method. In Fig. 6, (a) is the real profile of the work piece; (b) is the measurement obtained from this experimental method; (c) is the comparison between the real profile and the measurement from the positive direction of the $X$-axis. The solid line denotes the former while the dashed denotes the latter. It can be seen that these two curves coincide with each other well, which indicates that this method has considerable precision.

## 3. Experimental results and analysis

### 3.1. Reconstruction of fracture surface of concrete

A three-point bending, single edge-notched specimen with a notch/depth ratio of 0.50 was analyzed. The mix proportions of the concrete are given in Table 1. Dimensions of the specimen were: length × depth × width = 515 × 100 × 100 mm. In Fig. 7, the left figure is the photo of the original fracture surface of concrete, while the right one is the 3-D profile of the fracture surface measured by this technique. The color depth of the color bar was directly proportional to the depth variability measured. The darker the color, the more significant the depth variability. Com-

Table 1
Concrete mix proportions

| Cementitious materials | Water | Coarse aggregate | Sand | Water–binder ratio | Slump | Maximum size of coarse aggregate |
|---|---|---|---|---|---|---|
| 472 kg/m$^3$ | 168 kg/m$^3$ | 1110 kg/m$^3$ | 740 kg/m$^3$ | 0.44 | 18 cm | 16 mm |

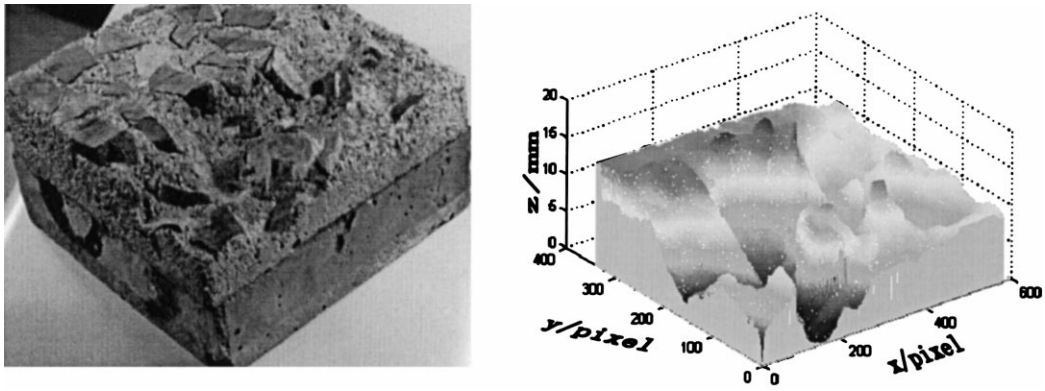


Fig. 7. Reconstruction of fracture surface of concrete.

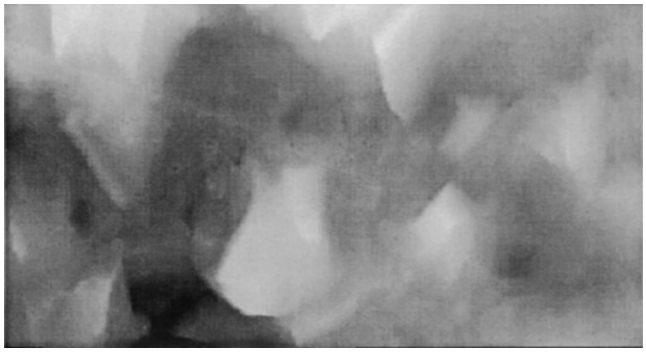

Fig. 8. An 8-bit grey image of the fracture surface of concrete.

paring these two figures, it can be seen that the details in the right figure are identical with those of the real photo.

### 3.2. Preliminary analysis of fracture surface

#### 3.2.1. Modified slit-island measurement

Fig. 8 showed the 8-bit grey image of the fracture surface of concrete; the grey value was directly proportional to the depth measured by laser triangulation. The ruptured aggregates in Fig. 7 (i.e. the bulgy parts) were brighter in the grey image, while the darker parts around them illustrated fracture along the aggregate–matrix interface. Therefore, the grey image can also qualitatively reflect the shape of the real fracture surface.

Different from the traditional slit-island method, the slit-island coastlines characterizing irregularities of fracture surfaces were generated without polishing the fracture surfaces in this work. By setting different grey threshold values, those pixels whose grey values were lower than

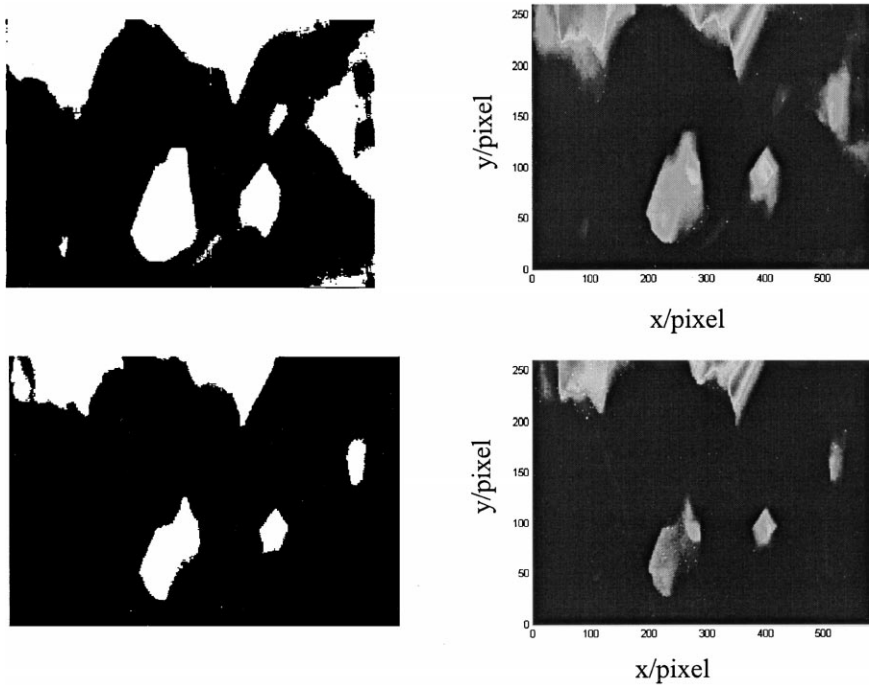


Fig. 9. Grey images at different grey values and real profiles.

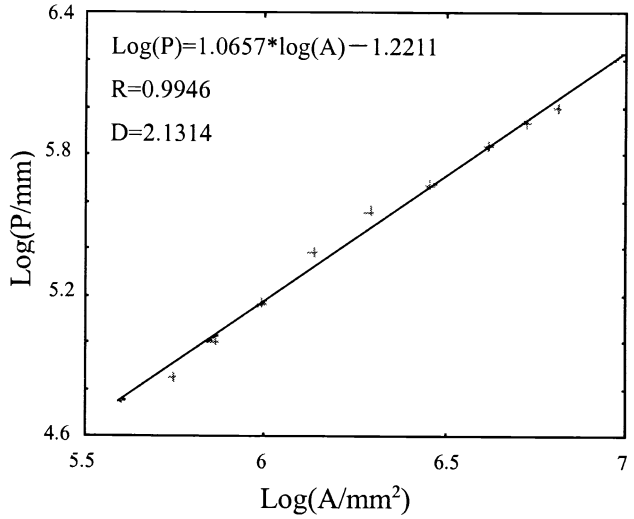


Fig. 10. The perimeter–area bilogarithmic diagram.

the threshold values were filtered and the binary images were generated. In Fig. 9, the left images are the binary images of threshold values of 150 and 180, respectively, while the right images are the corresponding vertical views of fracture surfaces. Measurements of the perimeters $P$ and areas $A$ of islands at different grey values were plotted on a logarithmic scale and fitted by linear regression (Fig. 10). The perimeter–area relationship can be described as Eq. (4):

$$P^{1/D} \propto A^{1/2}. \quad (4)$$

The fractal dimension $D$ was then obtained from equation (5):

$$\log(P) = C + \frac{D}{2}\log(A) \quad (C \text{ is the constant}). \quad (5)$$

The excellent linear relationship in the diagram indicates that the fracture surface was fractal, and the fractal dimension value $D$ was 2.1314, which agrees with the value obtained by other researchers [14].

Table 2
Fractal dimension of fracture surfaces

| Number | $D1$ | $R1$ | $D2$ | $R2$ | $D$ |
|---|---|---|---|---|---|
| 1 | 1.0539 | 0.9397 | 1.0490 | 0.9761 | 2.1029 |
| 2 | 1.0568 | 0.9508 | 1.0534 | 0.9880 | 2.1102 |
| 3 | 1.0513 | 0.9595 | 1.0707 | 0.9978 | 2.1220 |
| 4 | 1.0522 | 0.9280 | 1.0526 | 0.9788 | 2.1048 |
| 5 | 1.0429 | 0.9591 | 1.0564 | 0.9988 | 2.0993 |
| 6 | 1.0390 | 0.9309 | 1.0361 | 0.9967 | 2.0751 |
| Ave. | 1.0493 | 0.9447 | 1.0530 | 0.9894 | 2.1023 |

### 3.2.2. Vertical section measurement

Fig. 11 showed some section curves parallel to (a) and perpendicular to (b) the direction of the crack propagation.

Instead of actually sectioning the fracture surfaces, the section curves can be obtained from coordinates of the reconstructed fracture surfaces. The measurement results of the fractal dimension values $D1$ along the direction of the crack propagation, the fractal dimension values $D2$ perpendicular to the direction of the crack propagation and the total fractal dimension values $D = D1 + D2$ are given in Table 2. In this table, $R$ is the correlation coefficient of linear regression based on formula (5). The fractal dimension value measured by this method was 2.1023.

### 3.2.3. Roughness index measurement

The roughness index $R_s$ is defined as the ratio of the actual surface area to the projected surface [15]. In a micro-unit, $R_s$ is actually the reciprocal value of the cosine of the inclusion angle between the actual area and the projected area, $1/\cos\alpha_i$. The whole fracture surface consists of a number of micro-units and $R_s$ can be obtained by

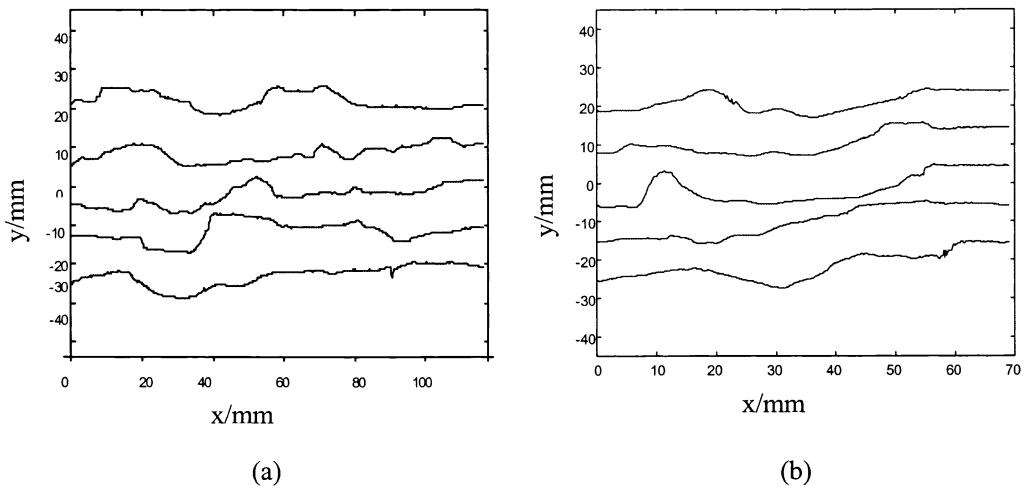


Fig. 11. Section curves of fracture surfaces.

accumulating and then averaging the total values of $1/\cos\alpha_i$. In this work, the value of $R_s$ is 1.4540. The true fracture surface area is about 45.4% greater than the nominal fracture area, which agrees with the conclusions in Ref. [3].

## 4. Conclusion

The advantage of laser triangulation by using a sheet beam and a plane-array CCD camera is that 2-D-scanning can be achieved by moving the object relative to the sensor only in one direction, so that the measuring system is simplified and can be operated conveniently. In this work, the fracture surface of concrete was characterized using laser triangulation to create the 3-D profile. Reconstruction of a standard work piece and a fracture surface of concrete showed that this technique has reasonable accuracy.

In the study, the profile reconstruction figure of a fracture surface is actually a combined figure, which consists of 200 sectioned contour lines. The shape of the fracture surface and the measurement of fractal dimension of the fracture surface can be achieved without any pretreatment such as polishing, sectioning the fracture surface, and so on. Moreover, through reconstructing the profile of the fracture surface, the details of the fracture surface at different scales can be obtained at will.

Preliminary analysis indicated that the fracture surface of concrete exhibits fractal characteristics. The fractal dimension $D$ varies from 2.0 to 2.2 and the value of roughness index $R_s$ showed that the true fracture surface area is about 45.4% greater than the nominal fracture area. However, due to the heterogeneity of concrete, the analysis of its fracture surface becomes more complicated.

## References

[1] A. Carpinteri, B. Chiaia, Multifractal nature of concrete surfaces and size effects on nominal fracture energy, Mater Struct 28 (1995) 435–443.
[2] A. Carpinteri, B. Chiaia, Crack-resistance behavior as a consequence of self-similar fracture topologies, Int J Fract 76 (1996) 327–340.
[3] B.B. Sabir, S. Wild, M. Asili, On the tortuosity of the fracture surface in concrete, Cem Concr Res 27 (5) (1997) 785–795.
[4] B.B. Mandelbrot, D.E. Passoja, A.J. Paullay, Fractal character of fracture surfaces of metals, Nature 308 (19) (1984) 721–722.
[5] H. Lin, Y. Li, Fractal Theory—Research on Singularity (in Chinese), The Publishing House of Beijing Polytechnical University, Beijing, 1992.
[6] M.A. Issa, A.M. Hammad, Assessment and evaluation of fractal dimension of concrete fracture surface digitized images, Cem Concr Res 24 (2) (1994) 325–334.
[7] N. Feng, High Performance Concrete (in Chinese), The Construction Industry Publishing House of China, Beijing, 1996.
[8] V.E. Saouma, C.C. Barton, N.A. Gamaleldin, Fractal characterization of fracture surface in concrete, Eng Frac Mech 35 (1990) 47–53.
[9] S. Diamond, S. Mindess, SEM investigation of fracture surfaces using stereo pairs: I. Fracture surfaces of rock and of cement paste, Cem Concr Res 22 (1) (1992) 67–78.
[10] T. Wada, R. Sato, C. Ishikawa, M. Ueda, New 2-dimensional analytical method for determination of the shape properties of concrete crack surfaces using a laser-beam, fracture mechanics of concrete structures, Proceedings FRAMCOS-3, 1998, pp. 293–304.
[11] W. Ren, P. Sun, Y. Wang, A calibration method for laser displacement system based on triangulation, Opt Technol (in Chinese) 3 (1997) 10–12.
[12] J. Zhang, B. Zhuang, C. Jiang, Q. Men, W. Zhang, Laser triangulation profile measurement (in Chinese), J Tianjin Univ 28 (2) (1995) 265–269.
[13] J. Hao, J. Zhao, H. Tan, E. Li, Method for improving precision of 3D-sensor based on laser triangulation (in Chinese), Opt Technol 2 (1998) 37–39.
[14] V.C. Saouma, C.C. Barton, Fractals, fractures and size effects in concrete, J Eng Mech ASCE 120 (4) (1994) 835–854.
[15] D.A. Lange, H.M. Jennings, S.P. Shah, Relationship between fracture surface roughness and fracture behavior of cement paste and mortar, J Am Ceram Soc 76 (3) (1993) 589–597.